Journal of Sound and Vibration (2000) **237**(2), 263–280
doi:10.1006/jsvi.2000.3027, available online at http://www.idealibrary.com on IDEAL®

DYNAMIC INTERACTION OF LONG SUSPENSION BRIDGES WITH RUNNING TRAINS

H. XIA

School of Civil Engineering, Northern Jiatong University, Beijing, China

AND

Y. L. XU AND T. H. T. CHAN

Department of Civil and Structural Engineering, The Hong Kong Polytechnic University, Hung Hom, Kowloon, Hong Kong, China. E-mail: ceylxu@polyu.edu.hk

(*Received* 27 *September* 1999, *and in final form* 29 *March* 2000)

This paper presents an investigation of dynamic interaction of long suspension bridges with running trains. A three-dimensional finite element model is used to represent a long suspension bridge. Each 4-axle vehicle in a train is modelled by a 27-degrees-of-freedom dynamic system. The dynamic interaction between the bridge and train is realized through the contact forces between the wheels and track. By applying a mode superposition technique to the bridge only and taking the measured track irregularities as known quantities, the number of degrees of freedom (d.o.f.) the bridge–train system is significantly reduced and the coupled equations of motion are efficiently solved. The proposed formulation and the associated computer program are then applied to a real long suspension bridge carrying a railway within the bridge deck. The dynamic response of the bridge–train system and the derail and offload factors related to the running safety of the train are computed. The results show that the formulation presented in this paper can well predict dynamic behaviors of both bridge and train with reasonable computation efforts. Dynamic interaction between the long suspension bridge and train is not significant.

1. INTRODUCTION

To meet the needs of modern society for advanced transportation systems more and more long suspension bridges carrying both highway and railway have been built throughout the world, such as the Minami Bisan Seto suspension bridge in Japan in 1988 [1] and the Tsing Ma suspension bridge in Hong Kong in 1997 [2]. For such long-span bridge–train systems, Diana and Cheli [3] pointed out the two fundamental aspects to be investigated: one is the bridge safety due to train passage and the other is the train runability including the passenger comfort. Compared with short-span railway bridges, long suspension bridges bear global deformation at very low frequency and local deformation at relatively high frequency. The vertical slopes related to the global deformation of the bridge deck and the lateral slopes of the bridge deck due to track eccentricities and irregularities should be limited to ensure train runability. The lateral forces given by wheels to track and the change of vertical forces on wheels and track should also be examined for train runability. On the other hand, periodic excitations caused by train passage generate local deformation and fatigue damage to bridge structural elements affecting bridge safety. In this connection, the mechanical model of a bridge–train system should be able to reproduce the details of bridge

0022-460X/00/420263 + 18 $35.00/0

characteristics, train complex configuration, and contact conditions between wheels and track. This demand, however, may be seriously constrained by the great computational effort required due to the large size of a suspension bridge and several locomotives and coaches travelling on the bridge at the same time.

Yasoshima *et al.* [4] thus studied first the behavior of the bridge under moving loads, and then analyzed the behavior of the train using the obtained responses of the track as inputs. This approach needs relatively less computational effort but it neglects the interaction between the train and the bridge. Diana and Cheli [3] used the direct numerical integration method to simultaneously solve the separated equations of motion of the train and bridge with constraints from the coupled conditions between the two subsystems. However, at each step of the time-domain analysis the iteration required having a convergent solution for the coupled system is time consuming. Another approach is to combine the two sets of equations of motion of both train and bridge and then to use the modal approach to find the solution [3]. In this approach, the mass, stiffness, damping, and contact force matrices of the system are time-dependent and of considerable size. Large computational efforts are thus unavoidable.

In this paper, a three-dimensional finite element model is used to represent a long suspension bridge. Each 4-axle vehicle in a train is modelled by a 27-d.o.f. dynamic system. The measured track irregularities and the wheel hunting described by a sinusoid function are used to represent the two most important self-excitations in the coupled train–bridge system. The degrees of freedom for all wheels are eliminated from the basic coupled equations of motion to reduce computation efforts. The mode superposition technique is then applied to the bridge only. This application further reduces computational efforts and also the modal damping values can be properly assigned. To examine the proposed formulation together with the associated computer program, a real long suspension bridge carrying a railway within the bridge deck is taken as a case study.

2. BASIC DYNAMIC MODELS

2.1. DYNAMIC MODEL OF TRAIN

A train usually consists of several locomotives, passenger coaches, freight cars, or their combinations. Each vehicle is in turn composed of a car body, bogies, wheel-sets, and the connections between the three components. To simplify the analysis but with enough accuracy, the following assumptions are used in the modelling of the train in this study:

(1) The car body, bogies and wheel-sets in each vehicle are regarded as rigid components, neglecting their elastic deformation during vibration (see Figure 1).
(2) The connections between the car body and a bogie are represented by two linear springs and two viscous dashpots of the same properties in either the horizontal direction or the vertical direction (see Figure 1). The stiffness and damping coefficients are denoted as k^h_{2ij} and c^h_{2ij} for the springs and dashpots in the jth bogie of the ith vehicle in the horizontal direction and k^v_{2ij} and c^v_{2ij} for the springs and dashpots in the jth bogie of the ith vehicle in the vertical direction.
(3) The connections between a bogie and a wheel-set are characterized as two linear springs and two viscous dashpots of the same properties in either the horizontal direction (k^h_{1ij} and c^h_{1ij}) or the vertical direction (k^v_{1ij} and c^v_{1ij}).

With the aforementioned assumptions, the ith vehicle has 5 d.o.f. They are designated by the lateral displacement Y_{ci}, roll displacement θ_{ci}, yaw displacement Ψ_{ci}, vertical

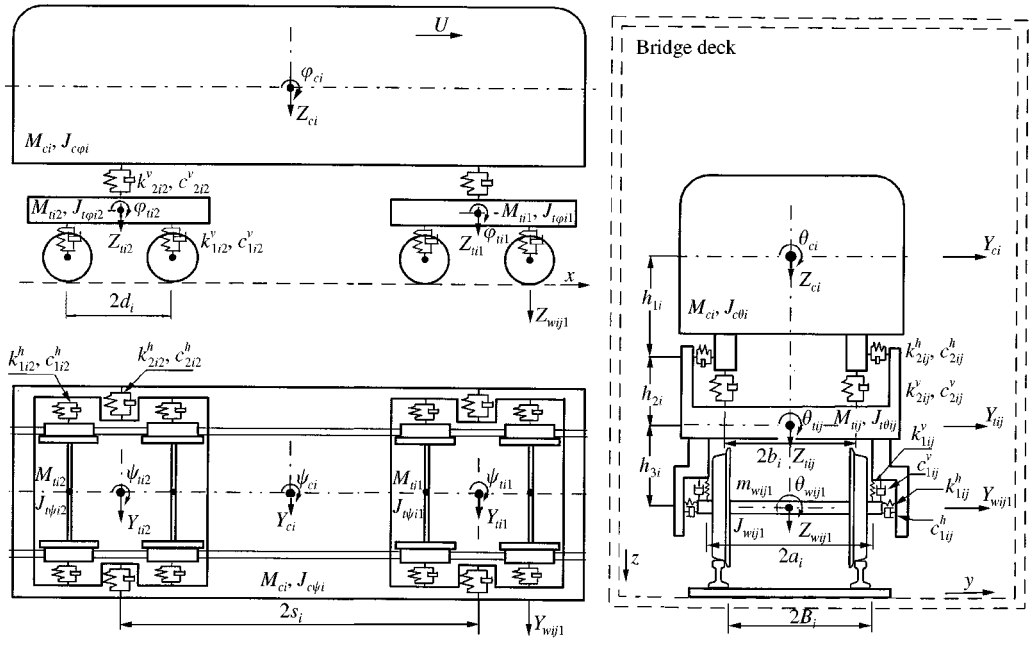

Figure 1. Dynamic model of vehicle.

displacement Z_{ci}, and pitch displacement φ_{ci}, all with respect to the earth. The jth bogie in the ith vehicle has 5 d.o.f.: the lateral displacement Y_{tij}, roll displacement θ_{tij}, yaw displacement Ψ_{tij}, vertical displacement Z_{tij}, and pitch displacement φ_{tij} with respect to the earth. For the lth wheel in the jth bogie and ith vehicle, only 3 d.o.f. are considered: the lateral displacement Y_{wijl}, roll displacement θ_{wijl}, and vertical displacement Z_{wijl} with respect to the earth.

For a 4-axle 2-bogie vehicle studied in this paper, the total d.o.f. are 27 (see Figure 1). By assuming that vibration amplitude of each component in a vehicle is small and using the equilibrium conditions, the equations of motion for the car body and two bogies in the ith vehicle can be derived as follows:

$$\begin{Bmatrix} \begin{bmatrix} \mathbf{M}_{cci} & 0 & 0 \\ 0 & \mathbf{M}_{t_1t_1i} & 0 \\ 0 & 0 & \mathbf{M}_{t_2t_2i} \end{bmatrix} \begin{Bmatrix} \ddot{\mathbf{v}}_{ci} \\ \ddot{\mathbf{v}}_{t_1i} \\ \ddot{\mathbf{v}}_{t_2i} \end{Bmatrix} + \begin{bmatrix} \mathbf{C}_{cci} & \mathbf{C}_{t_1ci} & \mathbf{C}_{t_2ci} \\ \mathbf{C}_{ct_1i} & \mathbf{C}_{t_1t_1i} & 0 \\ \mathbf{C}_{ct_2i} & 0 & \mathbf{C}_{t_2t_2i} \end{bmatrix} \begin{Bmatrix} \dot{\mathbf{v}}_{ci} \\ \dot{\mathbf{v}}_{t_1i} \\ \dot{\mathbf{v}}_{t_2i} \end{Bmatrix} \end{Bmatrix}$$

$$+ \begin{bmatrix} \mathbf{K}_{cci} & \mathbf{K}_{t_1ci} & \mathbf{K}_{t_2ci} \\ \mathbf{K}_{ct_1i} & \mathbf{K}_{t_1t_1i} & 0 \\ \mathbf{K}_{ct_2i} & 0 & \mathbf{K}_{t_2t_2i} \end{bmatrix} \begin{Bmatrix} \mathbf{v}_{ci} \\ \mathbf{v}_{t_1i} \\ \mathbf{v}_{t_2i} \end{Bmatrix} = \begin{Bmatrix} \mathbf{F}_{ci} \\ \mathbf{F}_{t_1i} \\ \mathbf{F}_{t_2i} \end{Bmatrix}, \tag{1}$$

where the subscripts c, t_1, t_2 represent the car body, the front and rear bogies of the vehicle, respectively, $i = 1, 2, \ldots, N_v$, and N_v is the number of vehicles on the bridge. The sub-mass, sub-damping, and sub-stiffness matrices are listed in Appendix A. $\dot{\mathbf{v}}_i$, $\dot{\mathbf{v}}_i$, and $\ddot{\mathbf{v}}_i$ are the displacement, velocity and acceleration vectors of the ith vehicle respectively. The force

vector consists of two parts:

$$\begin{Bmatrix} \mathbf{F}_{ci} \\ \mathbf{F}_{t_1 i} \\ \mathbf{F}_{t_2 i} \end{Bmatrix} = \begin{Bmatrix} \mathbf{F}_{cei} \\ \mathbf{F}_{t_1 ei} \\ \mathbf{F}_{t_2 ei} \end{Bmatrix} + \begin{Bmatrix} \mathbf{0} \\ \mathbf{F}_{t_1 wi} \\ \mathbf{F}_{t_2 wi} \end{Bmatrix}. \tag{2}$$

The components in the first part, $\mathbf{F}_{cei}$, $\mathrm{F}_{t_1 ei}$, and $\mathbf{F}_{t_2 ei}$ are the vectors of external forces (such as wind forces) acting on the car body, the front and rear bogies of the vehicle respectively. $\mathbf{F}_{t_1 wi}$ and $\mathbf{F}_{t_2 wi}$ are the vectors of forces transmitted from the wheels through the primary springs and dashpots to the front and rear bogies respectively. The forces transmitted from the wheels to the bogies can be expressed in terms of the displacements and velocities of the wheels.

$$F_{t_j wi} = \sum_{l=1}^{N_{wij}} \begin{cases} (k^h_{1ij} Y_{wijl} + c^h_{1ij} \dot{Y}_{wijl}) \\ 2a_i^2 (k^v_{1ij} \theta_{wijl} + c^v_{1ij} \dot{\theta}_{wijl}) - h_{4i} (k^h_{1ij} Y_{wijl} + c^h_{1ij} \dot{Y}_{wijl}) \\ 2\eta_l d_i (k^h_{1ij} Y_{wijl} + c^h_{1ij} \dot{Y}_{wijl}) \\ (k^v_{1ij} Z_{wijl} + c^v_{1ij} \dot{Z}_{wijl}) \\ 2\eta_l \mathrm{d}_i (k^v_{1ij} Z_{wijl} + c^v_{1ij} \dot{Z}_{wijl}) \end{cases} \quad j = 1, 2, \tag{3}$$

where N_{wij} is the number of wheel-sets in the jth bogie of the ith vehicle. η_l is the sign function with $\eta_l = 1$ when the wheel is in the front bogie and $\eta_l = -1$ when it is in the rear bogie. The explanation of the other terms in equation (3) can be found in Appendix A.

2.2. DYNAMIC MODEL OF SUSPENSION BRIDGE

A long suspension bridge consists mainly of bridge towers, bridge deck, cables, suspenders, and anchorages. When the bridge carries a railway, the track will be laid on the bridge deck and the forces from the wheels of a train will be transmitted to the bridge deck through the track. Since long suspension bridges are considered here, this study assumes that there is no relative displacement between the track and bridge deck. The elastic effects of the track system are also neglected. The suspension bridge is modelled as a three-dimensional system using the finite element method. The equation of motion for the bridge can be thus expressed as

$$\mathbf{M}\ddot{\mathbf{X}} + \mathbf{C}\dot{\mathbf{X}} + \mathbf{K}\mathbf{X} = \mathbf{F}, \tag{4}$$

where $\mathbf{M}$, $\mathbf{C}$, and $\mathbf{K}$ are the mass, damping and stiffness matrices of the bridge; $\ddot{\mathbf{X}}$, $\dot{\mathbf{X}}$, and $\mathbf{X}$ are the acceleration, velocity and displacement vectors of the bridge, respectively, and $\mathbf{F}$ is the force vector, consisting of two parts:

$$\mathbf{F} = \mathbf{F}_e + \mathbf{F}_w, \tag{5}$$

where $\mathbf{F}_e$ is the vector of external forces (such as wind forces) acting on the nodes of the bridge model, and $\mathbf{F}_w$ is the vector of forces from the wheels of a train on the bridge deck through the track (see Figure 2). The displacements of the bridge deck at any section in the finite element analysis are usually identified in terms of the lateral displacement Y_b, vertical displacement Z_b, and torsional displacement θ_b at the shear center (or centroid) of the cross-section. The lateral, vertical and torsional forces given by the lth wheel in the jth bogie of the ith vehicle corresponding to the deck displacements can be deduced in terms of the

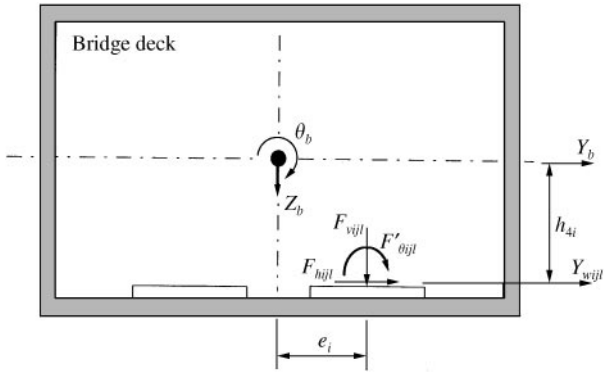

Figure 2. Vehicle forces on bridge deck.

equilibrium conditions of the wheel and the relative position of the track to the bridge deck cross-section as

$$F_{hijl} = -m_{wijl}\ddot{Y}_{wijl} + c^h_{1ij}(\dot{Y}_{t_ji} - h_{3i}\dot{\theta}_{t_ji} + 2\eta_l d_i\dot{\psi}_{t_ji} - \dot{Y}_{wijl}) + k^h_{1ij}(Y_{t_ji} - h_{3i}\theta_{t_ji} + 2\eta_l d_i\psi_{t_ji} - Y_{wijl}),$$

$$F_{vijl} = -m_{wijl}\ddot{Z}_{wijl} + c^v_{1ij}(\dot{Z}_{t_ji} + 2\eta_l d_i\dot{\varphi}_{t_ji} - \dot{Z}_{wijl}) + k^v_{1ij}(\dot{Z}_{t_ji} + 2\eta_l d_i\varphi_{t_ji} - \dot{Z}_{wijl}) + g[m_{wijl} + (0{\cdot}5M_{ci} + M_{t_ji})/N_{wij}],$$

$$F_{\theta ijl} = F_{\theta ijl} + h_{4i}F_{hijl} + e_iF_{vijl} = -J_{wijl}\ddot{\theta}_{wijl} + 2a_i^2c^v_{1ij}(\dot{\theta}_{t_ji} - \dot{\theta}_{wijl}) + 2a_i^2k^v_{1ij}(\theta_{t_ji} - \theta_{wijl}) + h_{4i}F_{hijl} + e_iF_{vijl}, \tag{6}$$

where m_{wijl} and J_{wijl} are the mass and the mass moment of the lth wheel, respectively, g is the acceleration due to gravity, and h_{4i} and e_i are the distances defined in Figure 2.

2.3. WHEEL HUNTING AND TRACK IRREGULARITIES

The deviations of the real rail from the ideal rail of perfect geometry are represented mainly by wheel hunting and track irregularity [5]. They are two important self-excitations in the bridge–train system in addition to the moving load of the train. In this study, the wheel hunting displacement (in the lateral direction) is assumed as a sinusoid function with a certain amplitude and a random phase:

$$Y_h(t) = A_h \sin\left(\frac{2\pi Ut}{L_h} + \phi_{hijl}\right), \tag{7}$$

where A_h is the hunting amplitude, L_h is the hunting wavelength, ϕ_{hijl} is the random phase of the lth wheel of the jth bogie in the ith vehicle ranging between 0 and 2π, and U is the speed of the train.

The track irregularities consist of the lateral irregularity $Y_s(x)$, vertical irregularity $Z_s(x)$, and rotational irregularity $\theta_s(x)$. In this study, the measured track irregularities are used so that these functions are regarded as known quantities. In consideration of both the wheel hunting and track irregularities, the relations between the lth wheel displacements and the

bridge deck displacements can be deduced as

$$\begin{Bmatrix} Y_{wijl} \\ \theta_{wijl} \\ Z_{wijl} \end{Bmatrix} = \begin{cases} Y_b(x_{ijl}) + h_{4i}\theta_b(x_{ijl}) + Y_s(x_{ijl}) + Y_h(x_{ijl}), \\ \theta_b(x_{ijl}) + \theta_s(x_{ijl}), \\ Z_b(x_{ijl}) + e_i\theta_b(x_{ijl}) + Z_s(x_{ijl}), \end{cases} \tag{8}$$

where x_{ijl} is the co-ordinate of the lth wheel of the jth bogie in the ith vehicle along the bridge deck.

3. EQUATIONS OF MOTION FOR BRIDGE–TRAIN SYSTEMS

This study concerns the dynamic interaction between the suspension bridge and train, and no external excitations such as wind or earthquake are included. Equations (1) and (3) for the train, equations (4) and (6) for the bridge, and equations (7) and (8) thus constitute the basic equations for the coupled bridge–train system. However, the direct integration of these equations in the time domain to find dynamic responses of both bridge and train is very cumbersome. The combination of these equations and then the application of mode superposition method are also very time consuming in the computation. Thus, this study applies the mode superposition method to the bridge only [6, 7]. The number of mode shapes of the bridge deck taken into account in the computation should be large enough to include the effects of both the global deformation of the bridge and the local deformation of the structural elements supporting the track. This decision may be made through a convergent study of the effects of the number of mode shapes or through a comparison with the measurement data. The mode shape between the deck nodes obtained from the eigenvalue analysis is determined using the Lagrange interpolation.

Let $\phi_h^n(x_{ijl})$, $\phi_\theta^n(x_{ijl})$ and $\phi_v^n(x_{ijl})$ denote, respectively, the values of the lateral, rotational and vertical components of the nth bridge mode at the position of the lth wheel of the jth bogie in the ith vehicle, and let q_n be the generalized co-ordinate of the nth mode. The displacement responses of the bridge deck at the same position can be expressed as

$$\begin{aligned} Y_b(x_{ijl}) &= \sum_{n=1}^{N_b} q_n \phi_h^n(x_{ijl}), \\ \theta_b(x_{ijl}) &= \sum_{n=1}^{N_b} q_n \phi_\theta^n(x_{ijl}), \\ Z_b(x_{ijl}) &= \sum_{n=1}^{N_b} q_n \phi_v^n(x_{ijl}), \end{aligned} \tag{9}$$

where N_b is the number of mode shapes concerned. If the mode shapes of the whole bridge are normalized based on $\{\phi^n\}^{\mathrm{T}} M \{\phi^n\} = 1$, the equation of motion of the bridge deck related to the nth mode can be derived based on equation (4) as

$$\ddot{q}_n + 2\xi_n \omega_n \dot{q}_n + \omega_n^2 q_n = F_n, \tag{10}$$

where ξ_n and ω_n are, respectively, the damping ratio and the circular frequency of the nth mode of the bridge, and F_n is the nth generalized force.

$$F_n = \sum_{i=1}^{N_y} \sum_{j=1}^{2} \sum_{j=1}^{N_{wij}} F_{nijl}, \tag{11}$$

where F_{nijl} is the nth generalized force from the lth wheel of the jth bogie of the ith vehicle,

$$F_{nijl} = \phi_h^n(x_{ijl})F_{hijl} + \phi_\theta^n(x_{ijl})F_{\theta ijl} + \phi_v^n(x_{ijl})F_{vijl}. \tag{12}$$

The expressions for the forces F_{hijl}, $F_{\theta ijl}$, and F_{vijl} can be found in equation (6). Furthermore, in terms of equation (9), the displacements of the lth wheel (see equation (8)) can be expressed as a function of the generalized co-ordinate and mode shape of the bridge as well as the known wheel hunting and track irregularities,

$$\begin{Bmatrix} Y_{wijl} \\ \theta_{wijl} \\ Z_{wijl} \end{Bmatrix} = \sum_{n=1}^{N_b} \begin{Bmatrix} q_n[\phi_h^n(x_{ijl}) + h_{4i}\phi_\theta^n(x_{ijl})] \\ q_n\phi_\theta^n(x_{ijl}) \\ q_n[\phi_v^n(x_{ijl}) + e_i\phi_\theta^n(x_{ijl})] \end{Bmatrix} + \begin{Bmatrix} Y_s(x_{ijl}) + Y_h(x_{ijl}) \\ \theta_s(x_{ijl}) \\ Z_s(x_{ijl}) \end{Bmatrix}. \tag{13}$$

Clearly, the displacements of the wheel need not be included in the equations of motion for the bridge–train system. This can reduce the computational effort significantly. Substituting equation (13) into equations (6) and (10)–(12) and also substituting equation (13) into equations (1)–(3), and then carrying out some manipulation, one can derive the coupled equations of motion for the bridge–train system as follows:

$$\begin{bmatrix} \mathbf{M}_{vv} & 0 \\ 0 & \mathbf{M}_{bb} \end{bmatrix} \begin{Bmatrix} \ddot{\mathbf{X}}_v \\ \ddot{\mathbf{X}}_b \end{Bmatrix} + \begin{bmatrix} \mathbf{C}_{vv} & \mathbf{C}_{vb} \\ \mathbf{C}_{bv} & \mathbf{C}_{bb} \end{bmatrix} \begin{Bmatrix} \dot{\mathbf{X}}_v \\ \dot{\mathbf{X}}_b \end{Bmatrix} + \begin{bmatrix} \mathbf{K}_{vv} & \mathbf{K}_{vb} \\ \mathbf{K}_{bv} & \mathbf{K}_{bb} \end{bmatrix} \begin{Bmatrix} \mathbf{X}_v \\ \mathbf{X}_b \end{Bmatrix} = \begin{Bmatrix} \mathbf{F}_v \\ \mathbf{F}_b \end{Bmatrix}, \tag{14}$$

where the subscripts "v" and "b" represent the vehicles and bridge respectively. The details of the submatrices in equation (14) can be found in Appendix B. Equation (14) is actually the second order linear non-homogeneous differential equation with time-varying coefficients. These equations are solved using the Newmark implicit integral algorithm with $\beta = 1/4$ in this study.

4. CASE STUDY

A computer program is written based on the formulation derived above and is used to perform a case study. The case study concerns a long suspension bridge carrying a railway inside the bridge deck (see Figures 3 and 4). The main span of the bridge is 1377 m and the height of the tower is 206 m, measured from the base level to the tower saddle. The two main cables of 36 m apart in the north and south are accommodated by the four saddles located at the top of the tower legs in the main span. On the right side, the main cables are extended from the tower saddles to the main anchorage through the splay saddles, forming a 300 m side span. On the left side, the main cables extended from the left tower are held first by the saddles on pier M2 at a horizontal distance of 355·5 m from the left tower and then by the main anchorage through splay saddles at the abutment. A three-dimensional finite element model of the bridge was established and the natural frequencies and mode shapes were computed. The computed natural frequencies and mode shapes were verified through the comparison with the measured results and the details can be found in reference [8]. The first 20 natural frequencies up to 0·38 Hz and the associated mode shapes are finally used in this case study since these natural frequencies and mode shapes have been validated against the measurement data. The accuracy of higher mode shapes from the computation depends on the detailed modelling of the deck structures, which are not included in this study. The damping ratios in the lateral and vertical modes of vibration are taken as 1% while the damping ratios in the torsional modes of vibration are 0·5%.

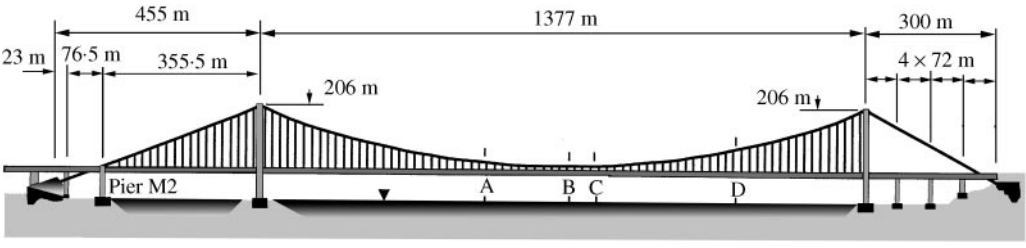

Figure 3. Configuration of suspension bridge used in the case study.

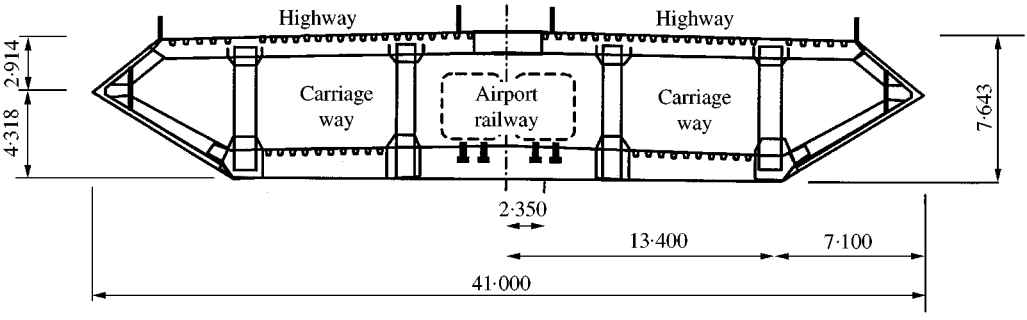

Figure 4. Typical cross-section of bridge deck.

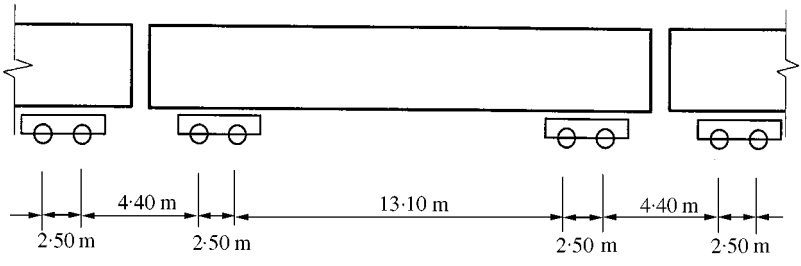

Figure 5. Configuration of train used in the case study.

The train concerned in the case study consists of eight passenger coaches. Each coach has two identical bogies and each bogie is supported by two identical wheel-sets (see Figure 5). The eight passenger coaches are assumed to be identical in this case study. The average static axle loads are 10 144 kg (tare) and 13 250 kg (crush). The main parameters of the coach used in the case study are listed in Table 1. The principal vibration mode frequency of the coach is about 1·04 Hz in the vertical direction and 0·68 Hz in the lateral direction.

The track vertical, lateral and torsional irregularities are taken into consideration by using the measured data from one of the main railways in China because no measurement data are available for the concerned bridge–train system. The length of the measured data is 2500 m and the samples of length 600 m are plotted in Figure 6(a) and (c) for vertical, lateral, and torsional irregularities respectively. Figure 7 displays the lateral track irregularity spectrum. It is seen that the spectrum is not a narrow spectrum and the significant

TABLE 1

Main parameters of vehicle used in the case study

Parameter	Unit	Value	Remarks
Full length of a coach (L)	m	22·5	
Distance between two bogies ($2s$)	m	15·6	
Distance between two wheel-sets ($2d$)	m	2·5	
Mass of car body (M_c)	t	50·99	Crush mass
Roll mass moment of car body ($J_{c\theta}$)	t m^2	154·83	Crush mass moment
Pitch mass moment of car body ($J_{c\varphi}$)	t m^2	1958·7	Crush mass moment
Yaw mass moment of car body ($J_{c\psi}$)	t m^2	1875·3	Crush mass moment
Mass of bogie (M_t)	t	4·36	
Roll mass moment of bogie ($J_{c\theta}$)	t m^2	1·47	
Pitch mass moment of bogie ($J_{c\varphi}$)	t m^2	3·43	
Yaw mass moment of bogie ($J_{c\psi}$)	t m^2	5·07	
Mass of wheel-set (m_w)	t	1·77	
Roll mass moment of wheel-set (J_w)	t m^2	0·92	
Primary vertical spring stiffness (k_1^v)	kN/m	2976	Each wheel-set
Primary lateral spring stiffness (k_1^h)	kN/m	20000	Each wheel-set
Secondary vertical spring stiffness (k_2^v)	kN/m	1060	Each bogie
Secondary lateral spring stiffness (k_2^h)	kN/m	460	Each bogie
Primary vertical dashpot (c_1^v)	kN s/m	15	Each wheel-set
Primary lateral dashpot (c_1^h)	kN s/m	15	Each wheel-set
Secondary vertical dashpot (c_2^v)	kN s/m	30	Each bogie
Secondary lateral dashpot (c_2^h)	kN s/m	30	Each bogie
Distance (h_1)	m	0·98	
Distance (h_2)	m	0·36	
Distance (h_3)	m	0·07	
Distance (h_4)	m	1·25	
Distance (a)	m	0·98	
Distance (b)	m	1·12	
Distance (B)	m	1·435	
Distance (e)	m	2·05	

excitation energy ranges between 5·0 and 40·0 m. The effect of wheel hunting displacement on both bridge and vehicle responses is so small that it is neglected in this case study.

4.1. RESPONSE OF BRIDGE

Displayed in Figure 8(a) and 8(b) are the time histories of the lateral displacement and acceleration responses of the bridge at the middle main-span, respectively, when the train runs on the bridge at a constant velocity of 70 km/h. It is seen from the response time histories that when the train runs on the left-side span, the bridge responses at the middle main-span are quite small. When the train travels on the main span, the bridge responses at the middle main-span become large. As the train travels on the right-side span, the bridge responses decrease. The bridge then has a free vibration when the train leaves from the bridge. Clearly, both the lateral displacement and acceleration responses of the bridge are quite small. Considering that track irregularities are the only excitation source to the bridge from the train, it can be thus concluded that the bridge lateral responses due to track irregularities are not significant.

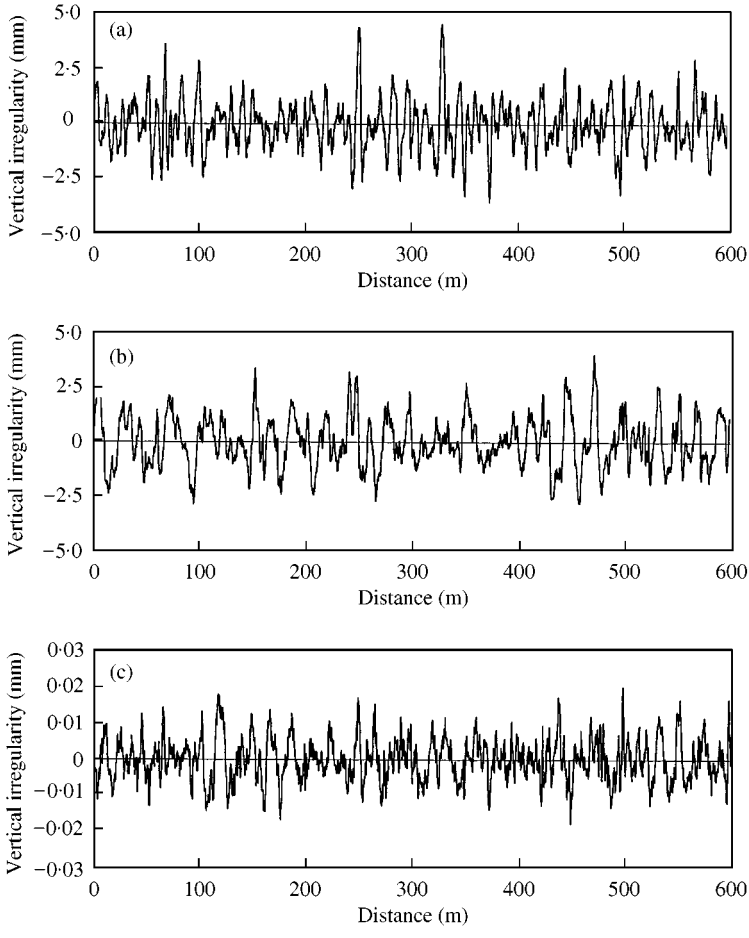

Figure 6. Measured track irregularity curves used in the case study: (a) lateral irregularity; (b) vertical irregularity; (c) torsional irregularity.

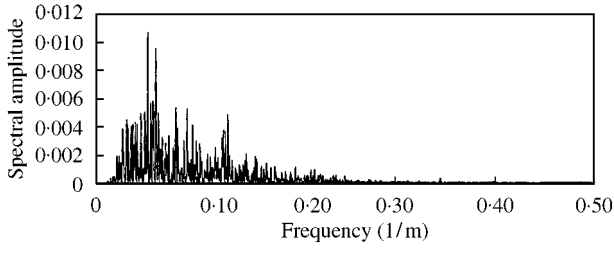

Figure 7. Track lateral irregularity spectrum.

Figure 9(a) shows the vertical displacement response of the bridge at four different positions. The distance of points A, B, C, and D from the left abutment of the bridge are, respectively, 1012·5, 1138·0,. 1174·0 and 1498·5 m. Points B and C are around the middle main-span. Point D is around the quarter of the main span from the right tower while point

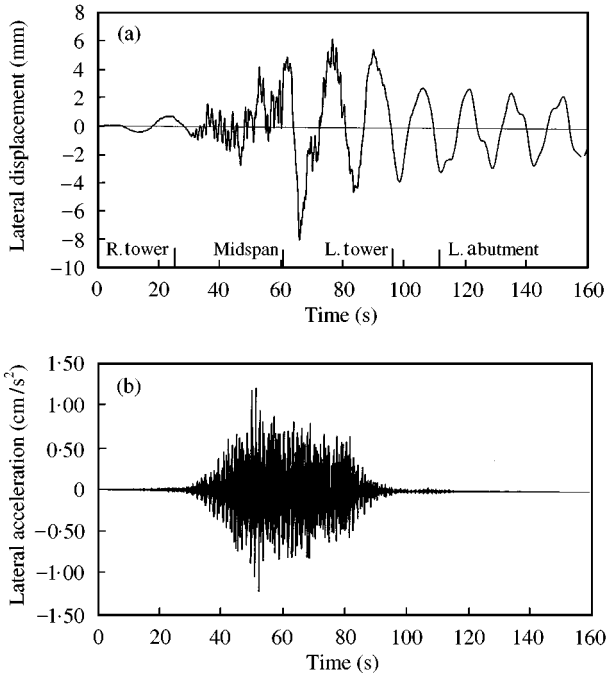

Figure 8. Lateral dynamic response of bridge at middle main spain: (a) lateral displacement response; (b) lateral acceleration response. $U = 70$ km/h.

A is at about 560 m from the left tower. All the vertical displacement responses are small when the train runs on the left- and right-side spans. The maximum vertical displacement response at each point occurs almost when the train runs around that point. The pattern of the displacement response, however, depends on the position concerned. For instance, the displacement response curves of points A and D are clearly different from those at positions B and C. It is also seen that the maximum response at point D is larger than that at point C, which may be because the first vertical mode of vibration of the bridge is almost anti-symmetrical. Although the maximum vertical displacement response at point C reaches 0·5 m, it is still very small compared with the main span of 1377 m length. This may be because the bridge is a low-frequency system while the train is a high-frequency system. Also, because the bridge is relatively long and the train is relatively light, the vertical dynamic displacement response looks like the static influence line.

Displayed in Figure 9(b) is the vertical acceleration response of the bridge at point C. It is seen that when the train runs on the main span, the higher-frequency component of the response due to the track irregularities appears in addition to the response component due to the passage of the train. The track irregularities, however, do not affect the vertical acceleration response of the bridge at the middle main span when the train runs on the side spans. This indicates that the effect of vertical track irregularity on bridge response is local. Clearly, the vertical acceleration response of the bridge due to the train is also not significant.

The bridge responses at four points are also computed for the train running at different speeds. The maximum lateral and vertical displacements and acceleration responses of the bridge at the four positions are listed in Table 2. It is seen that the maximum vertical displacement response, the maximum lateral acceleration response, and the maximum

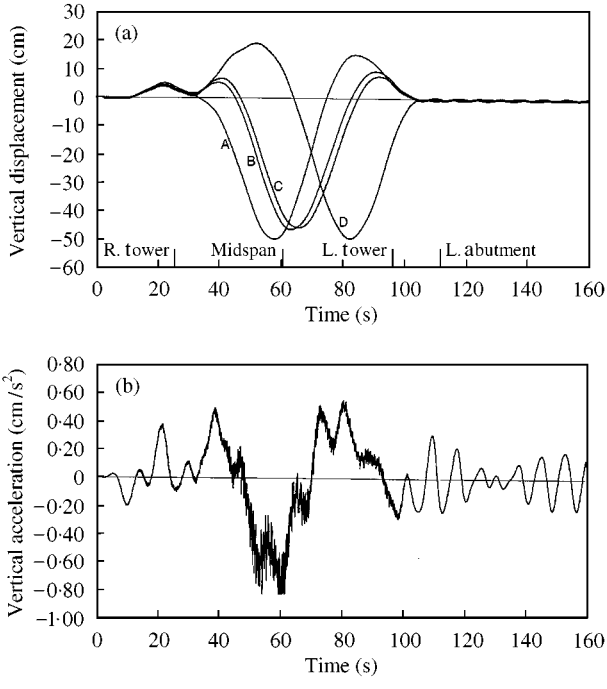

Figure 9. Vertical dynamic response of bridge at middle main spain: (a) vertical displacement response; (b) vertical acceleration response. $U = 70$ km/h.

vertical acceleration response of the bridge increase with the increasing train speed but the maximum lateral displacement response decreases with the increasing train speed.

4.2. RESPONSE OF VEHICLES

Figures 10 and 11 show, respectively, the lateral and vertical acceleration responses of the first car body in the train that runs on the bridge at a speed of 70 km/h. It is seen that the vertical response of the car body is only slightly larger than the lateral response but the patterns of the response time histories are different to some extent. The maximum acceleration responses in both directions are well below the allowable accelerations related to human comfort. It is also found that the lateral and vertical responses of the car body as the vehicles run on the bridge are similar to those when the vehicles run on the ground. This indicates that the motion of the long-span bridge does not affect the human comfort of vehicles. As a result, the track irregularities dominate the responses of the car body and these responses seem to be random signals.

There are two important parameters that should be considered in the evaluation of the safety of the train. One is the derail factor defined as the ratio of lateral force Q acting on the wheel-set to the total vertical force P acting on the same wheel-set. The total vertical force is the sum of the self-weight of the vehicle per wheel-set P_s and the dynamic vertical force P_d on the wheel-set. The other parameter is the offload factor defined as the ratio of the vertical force difference ΔP to the total vertical force P acting on the wheel-set with $\Delta P = P_s - P_d$. From the computed time histories of the derail factor and offload factor of the first wheel-set

TABLE 2

Maximum responses of bridge and vehicles

Types of response	Unit	$U = 20$ km/h	$U = 40$ km/h	$U = 70$ km/h	$U = 120$ km/h
Deck vertical displacement	cm	49·39	49·52	51·29	54·04
Deck vertical acceleration	cm/s^2	0·0845	0·332	0·878	3·156
Deck lateral displacement	mm	15·07	10·83	8·058	4·686
Deck lateral acceleration	cm/s^2	0·931	1·097	1·298	2·234
Vehicle vertical acceleration	cm/s^2	12·96	31·85	48·29	74·31
Vehicle lateral acceleration	cm/s^2	19·01	38·19	40·05	51·92
Derail factor	Q/P	0·247	0·287	0·306	0·413
Offload factor	$\Delta P/P$	0·380	0·381	0·393	0·410

Note: U is the train speed.

in the first vehicle of the train travelling at a speed of 70 km/h, it is found that the value of derail factor ranges from $-0{\cdot}27$ to $+0{\cdot}32$. The maximum value of derail factor is thus well below the allowable value of 0·80 specified in the Chinese code. It is also found that the amplitude of offload factor changes from $-0{\cdot}40$ to $+0{\cdot}37$ and its maximum value is also smaller than the allowable value of 0·6 specified in the Chinese code. The derail factor and the offload factor obtained as the vehicles run on the bridge are similar to those obtained as the vehicles run on the ground. Thus, the motion of the long-span suspension bridge does not significantly affect the runability of the vehicles in this case study.

The train acceleration responses and two factors are also computed for other train speeds. The maximum responses and the maximum values of the two factors are listed in Table 2. It is seen that the train responses increase significantly with the increasing train speed. The increase of two factors, however, is relatively smaller with the increasing train speed.

5. CONCLUSIONS

A formulation has been presented in this paper for investigating the dynamic interaction of a long suspension bridge with running trains. Each railway vehicle was modelled as a 27-d.o.f. dynamic system and the suspension bridge was represented by a three-dimensional dynamic finite element model. To reduce the d.o.f. of the coupled bridge–train system, this study took the measured track irregularities as known quantities and applied the mode superposition technique to the bridge. A real long suspension bridge carrying train inside the bridge deck was taken as a case study. The dynamic response of the bridge–train system and the derail factor and offload factor related to the running safety of the train were computed. The results showed that the formulation presented in this paper could well predict dynamic behaviors of both bridge and train with reasonable computation efforts. It was also found that the dynamic responses of the long suspension bridge under running train are relatively small and the effects of the bridge motion on the runability of railway vehicles are insignificant. This, however, may not be true if the effect of strong wind on both bridge and vehicles is included.

It should also be pointed out that by using the mode superposition technique it is assumed that the bridge is operating in a linear range. This is acceptable in this study because the maximum displacement response of the bridge is much smaller than the bridge

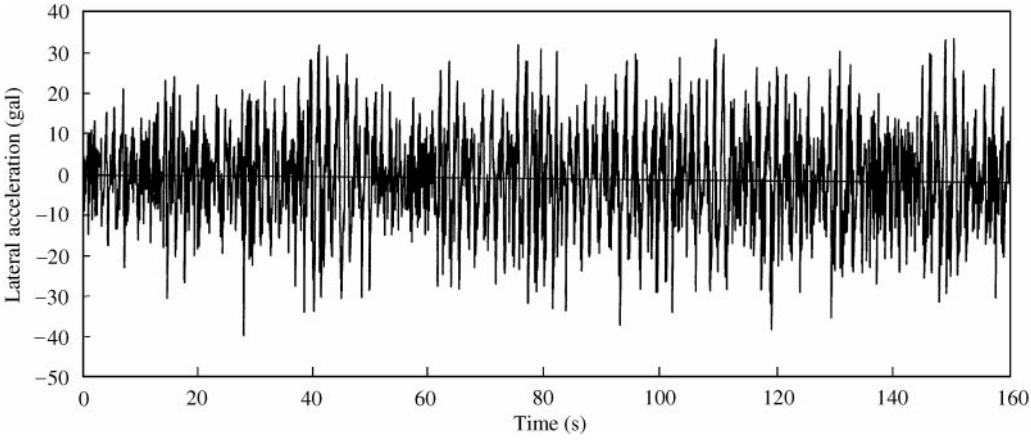

Figure 10. Lateral acceleration response of first car body.

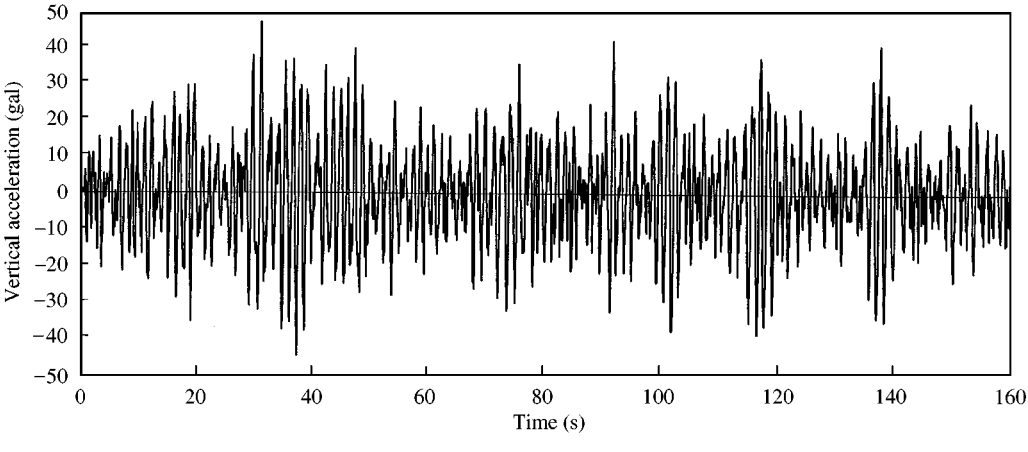

Figure 11. Vertical acceleration response of first car body. $U = 70$ km/h.

span. This assumption may not be acceptable when studying the problem of bridge–vehicle interaction under strong winds.

ACKNOWLEDGMENTS

The writers are grateful for the financial support from the Natural Science Foundation of China through an NSF grant and from the Hong Kong Polytechnic University through an internal research grant. The support from the MTR Corporation Hong Kong Limited to provide the writers with the relevant vehicle information is particularly appreciated.

REFERENCES

1. N. J. GIMSING 1997 *Cable Supported Bridges*. Chichester, England: John Wiley & Sons.

2. A. S. BEARD and J. S. YOUNG 1995 *Proceedings of International Conference on Bridges into the* 21*st Century*, 93–100. Impressions Design & Print Ltd., Hong Kong, Aspects of the design of the Tsing Ma Bridge.
3. G. DIANA and F. CHELI 1989 *Vehicle System Dynamics* **18**, 71–106. Dynamic interaction of railway systems with large bridges.
4. Y. YASOSHIMA, Y. MATSUMOTO and T. NISHIOKA 1981 *Journal of Faculty of Engineering Tokyo University Japan* **XXXVI**. Studies on the running stability of railway vehicles on a suspension bridge.
5. L. FRYBA 1996 *Dynamics of Railway Bridges*. London, England: Thomas Telford.
6. H. XIA and Y. J. CHEN 1995 *Advances in Structural Engineering* (Xia and Chen, editors), 48–54. Beijing, China: China Railway Publishing House. Dynamic analysis of steel truss bridges under moving train loads.
7. H. XIA, H. XHANG and G. DE ROECK 1998 *Proceedings of* 4*th International Conference on Stochastic Structural Dynamics, Notre Dame, U.S.A.*, 535–542. Rotterdam: Balkema, Dynamic analysis of train–bridge system under random excitations.
8. Y. L. XU, J. M. KO and W. S. ZHANG 1997 *Journal of Bridge Engineering, ASCE*. **3**, 149–156. Vibrations studies on Tsing Ma suspension Bridge.

APPENDIX A. SUB-MATRICES IN EQUATION (1)

Each sub-mass matrix is a diagonal matrix, expressed as

$$M_{cci} = \text{diag}[M_{ci}\ J_{c\theta i}\ J_{c\psi i}\ M_{ci}\ J_{c\varphi i}], \tag{A1}$$

$$M_{t_j t_j i} = \text{diag}[M_{tij}\ J_{t\theta ij}\ J_{t\psi ij}\ M_{tij}\ J_{t\varphi ij}], \tag{A2}$$

where M_{ci}, $J_{c\theta i}$, $J_{c\psi i}$, and $J_{c\varphi i}$ are the mass, mass moment about the x-axis, mass moment about the z-axis, and mass moment about the y-axis of the car body of the ith vehicle respectively. M_{tij}, $J_{t\theta ij}$, $J_{t\psi ij}$ and $J_{t\varphi ij}$ are the mass, mass moment about the x-axis, mass moment about the z-axis, and mass moment about the y-axis of the jth bogie in the ith vehicle respectively. In this study, $j = 1, 2$.

The sub-stiffness matrices are expressed as

$$\mathbf{K}_{cci} = \begin{bmatrix} k^h_{2i1}+k^h_{2i2} & -(k^h_{2i1}+k^h_{2i2}) & 0 & 0 & 0 \\ -(k^h_{2i1}+k^h_{2i2}) & h^2_{1i}(k^h_{2i1}+k^h_{2i2})+b^2_i(k^v_{2i1}+k^v_{2i2}) & 0 & 0 & 0 \\ 0 & 0 & s^2_i(k^h_{2i1}+k^h_{2i2}) & 0 & 0 \\ 0 & 0 & 0 & k^v_{2i1}+k^v_{2i2} & 0 \\ 0 & 0 & 0 & 0 & s^2_i(k^v_{2i1}+k^v_{2i2}) \end{bmatrix}, \tag{A3}$$

$$\mathbf{K}_{t_j t_j i} = \begin{bmatrix} k^h_{2ij}+2k^h_{1ij} & h_{2i}k^h_{2ij}-2h_{3i}k^h_{1ij} & 0 & 0 & 0 \\ h_{2i}k^h_{2ij}-2h_{3i}k^h_{1ij} & h^2_{2i}k^h_{2ij}+b^2_i k^v_{2ij}+2h^2_{3i}k^h_{1ij}+2a^2_i k^v_{1ij} & 0 & 0 & 0 \\ 0 & 0 & 2d^2_i k^h_{1ij} & 0 & 0 \\ 0 & 0 & 0 & 2k^v_{1ij}+k^v_{2ij} & 0 \\ 0 & 0 & 0 & 0 & 2d^2_i k^v_{1ij} \end{bmatrix}, \tag{A4}$$

$$\mathbf{K}_{ct_1} = \mathbf{K}_{t_1c}^T = \begin{bmatrix} -k_{2i1}^h & h_{1i}k_{2i1}^h & -s_i k_{2il}^h & 0 & 0 \\ -h_{2i}k_{2i1}^h & h_{1i}h_{2i}k_{2i1}^h - b_i^2 k_{2i1}^v & -h_{2i}s_i k_{2i1}^h & 0 & 0 \\ 0 & 0 & 0 & 0 & 0 \\ 0 & 0 & 0 & -k_{2i1}^v & -s_i k_{2i1}^v \\ 0 & 0 & 0 & 0 & 0 \end{bmatrix}, \quad \text{(A5)}$$

$$\mathbf{K}_{ct_2} = \mathbf{K}_{t_2c}^T = \begin{bmatrix} -k_{2i2}^h & h_{1i}k_{2i2}^h & s_i k_{2i2}^h & 0 & 0 \\ -h_{2i}k_{2i2}^h & h_{1i}h_{2i}k_{2i2}^h - b_i^2 k_{2i2}^v & h_{2i}s_i k_{2i2}^h & 0 & 0 \\ 0 & 0 & 0 & 0 & 0 \\ 0 & 0 & 0 & -k_{2i2}^v & -s_i k_{2i2}^v \\ 0 & 0 & 0 & 0 & 0 \end{bmatrix}, \quad \text{(A6)}$$

where h_{ij}, h_{2i}, and h_{3i} are the vertical distances between the three components in the ith vehicle, as defined in Figure 1. a_i, b_i, d_i, and s_i are the longitudinal and lateral distances between various axes of the ith vehicle, as defined in Figure 1.

The sub-damping matrix can be obtained by simply replacing "k" in the corresponding sub-stiffness matrix by "c", $\mathbf{v}_i$, $\dot{\mathbf{v}}_i$, and $\ddot{\mathbf{v}}_i$ are the displacement, velocity and acceleration vectors of the ith vehicle respectively. As an example, the sub-displacement vectors for the car body and two bogies in the ith vehicle can be expressed as

$$\mathbf{v}_{ci} = [Y_{ci} \ \theta_{ci} \ \psi_{ci} \ Z_{ci} \ \varphi_{ci}]^{\mathrm{T}}, \quad \text{(A7)}$$

$$\mathbf{v}_{t_1 i} = [Y_{t_1 i} \ \theta_{t_1 i} \ \psi_{t_1 i} \ Z_{t_1 i} \ \varphi_{t_1 i}]^{\mathrm{T}}, \quad \text{(A8)}$$

$$\mathbf{v}_{t_2 i} = [Y_{t_2 i} \ \theta_{t_2 i} \ \psi_{t_2 i} \ Z_{t_2 i} \ \varphi_{t_2 i}]^{\mathrm{T}}. \quad \text{(A9)}$$

APPENDIX B. SUB-MATRICES IN EQUATION (14)

Assume that the number of vehicles on the bridge is N_v and the number of concerned vibration modes of the bridges is N_b, the sub-displacement vectors can be expressed as

$$\mathbf{X}_v = [\mathbf{X}_{v1} \ \mathbf{X}_{v2} \ \cdots \ \mathbf{X}_{vN_v}]^{\mathrm{T}}, \quad \mathbf{X}_b = [q_1 \ q_2 \ \cdots \ q_{N_b}]^{\mathrm{T}}, \quad \text{(B1)}$$

where $\mathbf{X}_{vi} = [\mathbf{v}_{ci}, \mathbf{v}_{t,i}, \mathbf{v}_{t_2 i}]^{\mathrm{T}}$ $i = 1, 2, \ldots, N_v$. The sub-mass and stiffness matrices of the vehicles are listed as follows:

$$\mathbf{M}_{vv} = \begin{bmatrix} \mathbf{M}_{v1} & 0 & 0 & 0 \\ 0 & \mathbf{M}_{v2} & 0 & 0 \\ 0 & 0 & \ddots & 0 \\ 0 & 0 & 0 & \mathbf{M}_{vN_v} \end{bmatrix}, \quad \mathbf{K}_{vv} = \begin{bmatrix} \mathbf{K}_{v1} & 0 & 0 & 0 \\ 0 & \mathbf{K}_{v2} & 0 & 0 \\ 0 & 0 & \ddots & 0 \\ 0 & 0 & 0 & \mathbf{K}_{vN_v} \end{bmatrix}, \quad \text{(B2)}$$

where

$$\mathbf{M}_{vi} = \begin{bmatrix} \mathbf{M}_{cci} & 0 & 0 \\ 0 & \mathbf{M}_{t_1 t_1 i} & 0 \\ 0 & 0 & \mathbf{M}_{t_2 t_2 i} \end{bmatrix}, \quad \mathbf{K}_{vi} = \begin{bmatrix} \mathbf{K}_{cci} & \mathbf{K}_{t_1 ci} & \mathbf{K}_{t_2 ci} \\ \mathbf{K}_{ct_1 i} & \mathbf{K}_{t_1 t_1 i} & 0 \\ \mathbf{K}_{ct_2 i} & 0 & \mathbf{K}_{t_2 t_2 i} \end{bmatrix}. \quad \text{(B3)}$$

The sub-damping matrix of the vehicle can be achieved by simply replacing "**K**" in the stiffness matrix by "**C**". The sub-mass, sub-stiffness, and sub-damping matrices of the bridge are deduced as follows:

$$\mathbf{M}_{bb} = \begin{bmatrix} 1 + M_b^{11} & M_b^{12} & \cdots & M_b^{1N_b} \\ M_b^{21} & 1 + M_b^{22} & \cdots & M_b^{2N_b} \\ \cdots & \cdots & \ddots & \cdots \\ M_b^{N_b 1} & M_b^{N_b 2} & \cdots & 1 + M_b^{N_b N_b} \end{bmatrix},$$

$$M_b^{nm} = \sum_{i=1}^{N_v} \sum_{j=1}^{2} \sum_{l=1}^{N_{wij}} (\Phi_{hijl}^{nm} m_{wijl} + \phi_{\theta ijl}^{nm} J_{wijl} + \Phi_{vijl}^{nm} m_{wijl}),$$

$$\mathbf{K}_{bb} = \begin{bmatrix} \omega_1^2 + K_b^{11} & K_b^{12} & \cdots & K_b^{1N_b} \\ K_b^{21} & \omega_2^2 + K_b^{22} & \cdots & K_b^{2N_b} \\ \cdots & \cdots & \ddots & \cdots \\ K_b^{N_b 1} & K_b^{N_b 2} & \cdots & \omega_b^{N_b} + K_b^{N_b N_b} \end{bmatrix},$$

$$K_b^{nm} = \sum_{i=1}^{N_v} \sum_{j=1}^{2} \sum_{l=1}^{N_{wij}} (\Phi_{hijl}^{nm} k_{1ij}^h + 2\phi_{\theta ijl}^{nm} k_{1ij}^v a_i^2 + \Phi_{vijl}^{nm} k_{1ij}^v),$$

$$\mathbf{C}_{bb} = \begin{bmatrix} 2\xi\omega_1 + C_b^{11} & C_b^{12} & \cdots & C_b^{1N_b} \\ C_b^{21} & 2\xi\omega_2 + C_b^{22} & \cdots & C_b^{2N_b} \\ \cdots & \cdots & \ddots & \cdots \\ C_b^{N_b 1} & C_b^{N_b 2} & \cdots & 2\xi\omega_{N_b} + C_b^{N_b N_b} \end{bmatrix},$$

$$C_b^{nm} = \sum_{i=1}^{N_v} \sum_{j=1}^{2} \sum_{l=1}^{N_{wij}} (\Phi_{hijl}^{nm} c_{1ij}^h + 2\phi_{\theta ijl}^{nm} c_{1ij}^v a_i^2 + \Phi_{vijl}^{nm} c_{1ij}^v), \tag{B4}$$

The sub-stiffness matrices attributed to the interaction between the bridge and the vehicles can be derived as follows:

$$\mathbf{K}_{vb} = \{\mathbf{K}_{bv}\}^{\mathrm{T}} = \begin{bmatrix} \mathbf{K}_{vb1} \\ \mathbf{K}_{vb2} \\ \cdots \\ \mathbf{K}_{vbN_v} \end{bmatrix}, \quad \mathbf{K}_{vbi} = \begin{bmatrix} 0 & 0 & \cdots & 0 \\ \mathbf{K}_{t_1 q 1}^i & \mathbf{K}_{t_1 q 2}^i & \cdots & \mathbf{K}_{t_1 q N_b}^i \\ \mathbf{K}_{t_2 q 1}^i & \mathbf{K}_{t_2 q 2}^i & \cdots & \mathbf{K}_{t_2 q N_b}^i \end{bmatrix},$$

$$\mathbf{K}_{tjqn}^i = \{\mathbf{K}_{qnt_j}^i\}^{\mathrm{T}} = -\sum_{l=1}^{N_{wij}} \begin{bmatrix} (\phi_{hijl}^h + h_{4i}\phi_{\theta ijl}^n) k_{1ij}^h \\ 2\phi_{\theta ijl}^n a_i^2 k_{1ij}^v - h_{4i}\phi_{hijl}^n k_{1ij}^h \\ 2\eta_l d_i \phi_{hijl}^n k_{1ij}^h \\ (\phi_{vijl}^h + e_i \phi_{\theta ijl}^n) k_{1ij}^v \\ 2\eta_l d_i \phi_{vijl}^n k_{1ij}^v \end{bmatrix}, \tag{B5}$$

where $i = 1, 2, \ldots, N_v$, $n = 1, 2, \ldots, N_b$, and $j = 1, 2$. The sub-damping matrices attributed to the interaction between the bridge and vehicles can be obtained by simply replacing "k" in equation (28) by "c". If the external forces such as wind and earthquake are not taken into account, the force vectors can be expressed as

$$\mathbf{F}_v = [\mathbf{F}_{v1} \;\; \mathbf{F}_{v2} \;\; \cdots \;\; \mathbf{F}_{vN_b}]^{\mathrm{T}}, \quad \mathbf{F}_b = [\mathbf{F}_{b1} \;\; \mathbf{F}_{b2} \;\; \cdots \;\; \mathbf{F}_{bN_b}]^{\mathrm{T}}, \quad \mathbf{F}_{vi} = \begin{bmatrix} 0 \\ \mathbf{F}_{vi}^{t1} \\ \mathbf{F}_{vi}^{t2} \end{bmatrix},$$

$$\mathbf{F}_{vi}^{ti} = \sum_{l=1}^{N_{wij}} \begin{cases} k_{1ij}^h [Y_s(x_{ijl}) + Y_h(x_{ijl})] + c_{1ij}^h [\dot{Y}_s(x_{ijl}) + \dot{Y}_h(x_{ijl})] \\ 2a_i^2 [k_{1ij}^v \theta_s(x_{ijl}) + c_{1ij}^v \dot{\theta}_s(x_{ijl})] - h_{4i} [k_{1ij}^h Y_s(x_{ijl}) + c_{1ij}^h \dot{Y}_s(x_{ijl})] \\ 2\eta_l d_i [k_{1ij}^h Y_s(x_{ijl}) + c_{1ij}^h \dot{Y}_s(x_{ijl})] \\ k_{1ij}^v Z_s(x_{ijl}) + c_{1ij}^v \dot{Z}_s(x_{ijl}) \\ 2\eta_l d_i [k_{1ij}^v Z_s(x_{ijl}) + c_{1ij}^v \dot{Z}_s(x_{ijl})] \end{cases}$$

$$(i = 1, 2, \ldots, N_v; j = 1, 2),$$

$$F_{bn} = \sum_{i=1}^{N_v} \sum_{j=1}^{2} \sum_{l=1}^{N_{wij}} \{(\phi_{hijl}^n + h_{3i}\phi_{hijl}^n) k_{1ij}^h Y_s(x_{ijl}) + 2\phi_{\theta ijl}^h k_{1ij}^v a_i^2 \theta_s(x_{ijl}) + \phi_{vij}^h k_{1ij}^v Z_s(x_{ijl})]$$
$$+ \phi_{vijl}^n g[m_{wijl} + (0{\cdot}5M_{ci} + M_{tij})/N_{wij}]\}, \tag{B6}$$

where

$$\Phi_{hijl}^{nm} = (\phi_{hijl}^n + h_{4i}\phi_{\theta ijl}^n)(\phi_{hijl}^m + h_{4i}\phi_{\theta ijl}^m), \quad \phi_{\theta ijl}^{nm} = \phi_{\theta ijl}^n \phi_{\theta ijl}^m \quad \text{and}$$
$$\Phi_{vijl}^{nm} = (\phi_{vijl}^n + e_i\phi_{\theta ijl}^n)(\phi_{vijl}^m + e_i\phi_{\theta ijl}^m).$$